Molecular Cell, Volume *32*

Supplemental Data

Hierarchical Regulation of WASP/WAVE Proteins

Shae B. Padrick, Hui-Chun Cheng, Ayman M. Ismail, Sanjay C. Panchal, Lynda K. Doolittle, Soyeon Kim, Brian M. Skehan, Junko Umetani, Chad A. Brautigam, John M. Leong, and Michael K. Rosen

Table S1. Proteins used in this work.

Construct	Protein sequence	Organism	Accession code and notes
WASP			
WASP VCA	421-502	Human	NM_000377
GST-WASP VCA	421-502	Human	
Rhodamine GST-WASP VCA	421-502	Human	Labeled on Cysteine in GST
FKBP-WASP VCA	WASP 421-502 FKBP 1-108	Human	WASP: NM_000377 FKBP: NP_463460
mTOR-WASP VCA	WASP 421-502 mTOR 2025-2114	Human	WASP: NM_000377 mTOR: NP_004949
xlWASP VCA	421-502	Human	Crosslinked using $BM(PEO)_3$ and CGGSGGSGGSGGS appended at the N-terminus.
N-WASP			
$N\text{-}WASP_C$	193-501	Rat	O08816
$N\text{-}WASP_C$*	193-501 (L232P)	Rat	
$N\text{-}WASP_B$	183-239+273-396	Rat	
$N\text{-}WASP_{BC}$*	183-239+273-501	Rat	
N-WASP VCA	393-505	Human	NM_003941
GST-N-WASP VCA	393-505	Human	

GST:GST-N-WASP VCA	393-505	Human	
Rhodamine N-WASP VCA (rVCA)	393-505	Human	C431A, C inserted at c-terminus for rhodamine labeling
N-WASP VCA RA/RA	393-505 (R414A,R442A)	Human	Prevents barbed end capture (Co et.al)
GST-N-WASP VCA RA/RA	393-505 (R414A,R442A)	Human	Prevents barbed end capture (Co et.al)
A488-N-WASP CA	465-505	Human	Alexa488 dye coupled to CGGSGGSGGSGGS appended at the N-terminus
WAVE1/Scar1			
WAVE1	1-559	Human	NM_003931
WAVE1ΔC	1-178	Human	
WAVE1 VCA	485-559	Human	
GST-WAVE1 VCA	485-559	Human	
Cortactin			
NtA	1-36	Human	NM_005231
rNtA	1-35	Human	Rhodamine dye coupled to Cys appended to N-term
A594-NtA	1-35	Human	Alexa594 dye coupled to Cys appended to N-term
EspFu			
EspFu 1R	268-314	EHEC	AB253537; fifth repeat
EspFu 2R	80-173	EHEC	First and second repeats
EspFu $2R_C$	221-314	EHEC	Fourth and fifth repeats
EspFu 5R	80-314	EHEC	Repeats 1-5
Nck			
Nck_F	109-253	Human	NM_006153
GST-Nck_F	109-253	Human	
GST:GSTNck_F	109-253	Human	
PACSIN2			
PACSIN2	1-486	Mouse	NP_035992
PACSIN2 SH3	420-486	Mouse	
GST-PACSIN2 SH3	420-486	Mouse	

Others			
Abi2	1-475	Human	BT009920
HSPC300	1-79	Human	AF161418 with 238C insertion in many ESTs
Cdc42	1-187	Human	NP_001034891
Arp2/3 complex		Bovine	
Actin		Rabbit	
Pyrene-Actin		Rabbit	

Generation of Materials

Proteins were expressed in *E. coli* strain BL21(DE3)T1^{R}. Bacteria were induced at OD_{600} 0.6 - 1.0 with 1 mM IPTG, and then grown either 3.5 hours at 37˚C or 16 hours at 20˚C. Cells were lysed by sonication or homogenization (EmulsiFlex-C5, Avestin) and lysates were cleared by centrifugation (50,000 g for 45 min). The only exception is the Abi2-WAVE1-HSPC300 heterotrimer and Abi2-WAVE1ΔC-HSP300 heterotrimer, see below for details. All columns and chromatography resins used in this work are from GE Healthcare, except NiNTA agarose (Qiagen) and Amylose resin (New England Biolabs).

N-WASP$_C$, N-WASP$_C$*

Proteins were expressed as Tev cleavable His_6 fusions, and purified over NiNTA agarose, and MonoQ. Following Tev cleavage at room temperature, they were desalted into MonoS binding buffer, purified over MonoS and then Superdex200pg in 150KMEI. Final material was used without concentration and N-WASP$_C$* was stored at concentrations above 1 μM for up to four days. N-WASP$_C$* was diluted to working concentrations 2 hrs before assays and assays were performed within 12 hrs.

N-WASP$_{BC}$*, N-WASP$_B$

Proteins were expressed as Tev cleavable His_6 fusions and purified over NiSepharoseFF. N-WASP$_{BC}$* was further purified over Source15Q. Materials were then cleaved with Tev protease at room temperature, then purified over Source15S and Superdex75.

GST-WASP VCA, GST-N-WASP VCA, GST-WAVE1 VCA, GST-N-WASP VCA RA/RA mutant, WASP VCA, N-WASP VCA, N-WASP VCA RA/RA mutant

Proteins were expressed as thrombin cleavable GST fusions, purified over DEAE SepharoseFF, GSH Sepharose 4B, MonoQ, and Superdex75pg in KMEI buffer and concentrated using YM10 Centriplus concentrators (Amicon). Free VCAs (WASP VCA, N-WASP VCA and N-WASP VCA RA/RA mutant) were produced by purification up to the MonoQ step above and then cleaved with thrombin (50U per liter of culture, 16 hours at 4˚C). Following thrombin cleavage, VCA was further purified over MonoQ (to remove thrombin and uncleaved material) and Superdex75pg in KMEI buffer, and then concentrated using YM3 Centriplus concentrators (Amicon). Mass spectrometry was performed on all free VCAs in this section to insure the integrity of their C-termini, since VCA activity decreases significantly with the loss of only 3 residues from the C-terminus. As purified here, the N-WASP and WASP VCAs have activity that is stable for > 1 week when stored at 4 °C, indicating a lack of C-terminal proteolysis in this timeframe. Mass spectrometry was performed by the Protein Chemistry Technology Center at UT Southwestern Medical Center at Dallas.

FKBP-WASP VCA

Protein was expressed as a His_6 fusion, and purified using NiSepharoseFF, Source15Q and Superdex75pg (in KMEI buffer).

mTOR-WASP VCA

Protein was expressed as a Tev cleavable GST fusion, and purified using GSH Sepharose 4B and Source15Q, cleaved using Tev protease at 4˚C. Cleaved protein was further purified using Source15Q and finally using Superdex75pg in KMEI buffer.

GST-Nck_F, GST-PACSIN2 SH3, Nck_F, PACSIN2 SH3

Proteins were expressed as Tev cleavable GST fusions and purified over GSH Sepharose 4B, MonoQ and Superdex75pg in KMEI. Cleaved materials (Nck_F and PACSIN2 SH3) were produced by purification to the MonoQ step above, then cleaved with Tev protease for 16 hours at 4˚C. Following cleavage, materials were further purified over Source15Q (to remove Tev and uncleaved material) and Superdex75pg in KMEI buffer, and concentrated using a 5K cutoff AmiconUltra15 (Amicon).

GST:GST-N-WASP VCA, GST:GST-Nck_F

Free GST was expressed from an unmodified pGEX2T vector and purified following the method used for GST-Nck_F. Purified GST was mixed at a 10:1 molar ratio (in KMEI) with GST-N-WASP VCA or GST-Nck_F and incubated 16 hours at 4˚C. Immediately before use in activity assays small quantities of the mixture were purified over Source15Q at pH 6 (to separate heterodimers from homodimers), then buffer exchanged into KMEI using a 5ml HiTrap Desalting column. Final materials were used without

concentration and within 15-45 minutes of beginning purification, as appreciable evidence of back exchange is observed within three hours of preparation.

PACSIN2

Protein was expressed as a thrombin cleavable GST fusion, and purified over GSH Sepharose 4B, desalted, and then cleaved with thrombin (50U per liter of culture, 16 hours at 4˚C). Cleaved protein was further purified using GSH Sepharose 4B and Superdex200pg in KMEI and concentrated using an AmiconUltra15, 30K cutoff.

xlWASP VCA, C(GGS)$_4$WASP VCA

WASP VCA protein was expressed as a Tev cleavable GST fusion with CGGSGGSGGSGGS appended at the N-terminus. Material was purified over DEAE SepharoseFF, GSH Sepharose 4B, then cleaved with Tev protease. Cleaved material was then purified over MonoQ using pH 7 imidazole buffer without reducing agent and immediately crosslinked at 22˚C for one hour using a 1.2 fold excess of BM(PEO)$_3$ (Pierce) added in four aliquots. Following crosslinking, dimeric material was resolved from mono-VCA material using Source15Q. Finally, material was passed over Superdex75pg into KMEI and concentrated using YM3 Centriplus concentrators (Amicon). The monomeric version, C(GGS)$_4$WASP VCA, was produced by Tev cleaving following the GSH Sepharose step purifying by MonoQ and Superdex75pg into KMEI. ^{15}N labeled materials were produced by expressing the proteins in M9 media containing ^{15}N labeled ammonium chloride.

NtA, rNtA, A594-NtA

The cortactin NtA domain was expressed as a Tev cleavable GST fusion. Material was purified over GSH Sepharose 4B then cleaved with Tev protease at room temperature. Cleaved material was then purified over Source15Q. Finally, material was passed over Superdex75pg into KMEI. Fluorescently labeled materials were expressed with an added amino-terminal cysteine. These were purified over GSH Sepharose 4B, then over Source15Q in pH 7 imidazole buffers lacking reducing agent. 10mM EDTA and a five-fold excess of tetramethylrhodamine (Invitrogen #T6027) or Alexa594 (Invitrogen #A10256) maleimide in DMSO were added and incubated at 4˚C for 12 hours. The reaction was quenched with 2mM DTT and excess dye was removed by purification over Source15Q. Finally, material was purified over Superdex75 into KMEI. Mass spectrometry of the final material showed no signs of unreacted material. Concentrations were measured using amino acid analysis (Keck Center, Yale).

A488-N-WASP CA

The CA region of N-WASP was expressed as a Tev cleavable fusion to GST with an amino terminal CGGSGGSGGSGGS appended. Material was purified over DEAE SepharoseFF, then GSH Sepharose 4B and cleaved with Tev protease at room temperature and purified using MonoQ. Prior to labeling it was passed over Source15Q in pH 7 imidazole buffer lacking reducing agent. 10mM EDTA and a five-fold excess of Alexa488 maleimide (Invitrogen #A10254) were added and reacted at 4˚C for 12 hours. The reaction was quenched with 2mM DTT and excess dye was removed by centrifugation and purification over Source15Q and Superdex75. Mass spectrometry of the final material showed no signs of unreacted material. Concentrations were measured

using amino acid analysis (Keck Center, Yale). ~97% Photobleached material was generated by exposing a stock of A488-N-WASP CA to the beam from a solid state laser (Sapphire 488-200, Coherent) for 45 minutes.

Abi2-WAVE1-HSPC heterotrimer, Abi2-WAVE1ΔC-HSPC heterotrimer

Baculoviruses to express Tev cleavable His_6-Abi2 and His_6-WAVE1, and Tev cleavable GST-HSPC were produced using the Bac-to-Bac system (Invitrogen). Sf9 cells were co-infected with the three baculoviruses. Sixty hours post infection, cells were harvested by centrifugation and lysed by 1 cycle of slow freeze/thaw. Lysate was cleared by centrifugation (50,000 g for 45 min). The complex was purified over NiNTA agarose, GSH Sepharose 4B, cleaved with TEV protease at 4°C, then purified over Source15Q and Superose6. Twenty percent glycerol was added to all buffers to prevent precipitation and aggregation of the complex. To produce a heterotrimer lacking the WAVE1 VCA, His_6-Abi2 was expressed in insect cells and purified from cleared lysate over NiNTA agarose; MBP-HSPC300 and MBP-WAVE1ΔC (WAVE1 lacking the polyproline region and VCA) were expressed in bacteria and purified from cleared lysate over amylose affinity resin. HSPC300 was further purified over Source15Q. The three proteins were then incubated together in the presence of 1% Nonidet P-40 for 48 hours. The resulting complex was further purified over Source15Q, amylose resin and finally Superdex200.

PIP_2 Vesicles

PIP_2 vesicles were prepared following established protocols (Ho et al., 2006). Briefly, phosphotidyl-choline (Avanti, #840051C), phosphatidyl-inositol (Avanti, #840042C) and $PIP(4,5)_2$ (Avanti, #840046X) were purchased as prepared solutions in organic solvent.

Appropriate quantities of the lipid solutions were mixed in glass tubes and dried under a stream of argon and then under vacuum for at least three hours. Dried lipid films were hydrated in KMEI for 30 minutes at 22˚C, then freeze thawed in liquid nitrogen for five cycles and left at -80˚C until ready for use. Frozen lipids were thawed and extruded through 100 nm pore size polycarbonate membranes (Avanti) for at least 21 passes. Lipid suspensions were then stored at 4˚C and used within 24 hours to minimize loss of inositol phosphate headgroups. Suspensions were warmed to 22 ˚C shortly before use in assays. Density of PIP_2 was controlled by mixing different quantities of PIP_2 into an equimolar mix of phosphotidyl-choline and phosphatidyl-inositol in solvent prior to drying. Carrier lipid vesicles are an equimolar mix of phosphotidyl-choline and phosphatidyl-inositol reconstituted using the same method.

Other Materials

Bovine Arp2/3 complex (Higgs et al., 1999), rabbit skeletal muscle actin and pyrene-actin (Cooper and Pollard, 1982), Cdc42 (Leung et al., 2006), WAVE1 VCA, rhodamine-labeled N-WASP VCA (Panchal et al., 2003), EspFu 1R, 2R and 5R (Cheng et al., 2008) were purified as described previously. Arp2/3 complex was stored at 4 °C and used within three weeks of purification for actin polymerization assays and within 1 week for affinity measurements.

Analytical Ultracentrifugation

Raw absorbance and interference concentration profiles obtained from the sedimentation velocity (SV) experiments were fit using continuous $c(s)$ distributions, which were further analyzed to yield masses as described in the main text. Analyses presented in Figure 2A were performed with identical s-value ranges to ensure uniformity. The following details the parameters used and their values. A resolution of 50 s-values ranging from 2.0 to 15 S were considered. Values for partial specific volume ($\bar{v}$), buffer density (ρ), and buffer viscosity (η) were estimated by extrapolating literature values, as implemented in SEDNTERP (Laue et al., 1992). Because the optima for frictional ratio (f/f_0), baseline, time-independent noise, and sample meniscus are not available through simple least-squares minimization, their values were optimized using an iterative simplex routine. The radial value for the bottom of the cell was held fixed at 7.2 cm. To avoid artificial high-frequency oscillations in the distributions, the information content of the distributions was reduced using the maximum-entropy regularization protocol (Schuck, 2000) such that the reported distributions had r.m.s.d.'s within 1 σ (i.e. an F-ratio of 0.68) of the best-fit distributions. Once the fit had converged on a minimum r.m.s.d. value, the resolution was increased to 150 s-values for calculation of the final $c(s)$ distributions as presented.

The mass for the complex between GST-WASP VCA and Arp2/3 complex was obtained using a bimodal $c(s)$ distribution in SEDFIT. In the above analyses, a single f/f_0 was refined for the entire $c(s)$ distribution. However, the GST-VCA dimer and Arp2/3 have significantly different f/f_0's (1.63 for the former, 1.37 for the latter), invalidating the

underlying assumption of frictional-ratio uniformity. In studies featuring a heterogeneous mixture of species with different f/f_0's, the species whose experimental signal is greatest tends to dominate the refinement of the frictional ratio (Brown and Schuck, 2006). Indeed, this is the case with a mixture of GST-VCA dimer (3.0 μM) and Arp2/3 (0.4 μM): the refined f/f_0, 1.65, is very close to that of GST-VCA alone. It is therefore justifiable to take a different approach in analyzing such mixtures. The distribution of *s*-values was divided into two domains, and separate f/f_0's were refined for each domain. Domain 1 was defined as 2.0 S < *s* < 9.0 S plus 13.0 S < *s* < 15.0 S, which should cover GST-VCA alone and any aggregated species. Domain 2 was defined as 9.0 S ≤ *s* ≤ 13.0 S, the range in which we observe cosedimentation of the GST-VCA:Arp2/3 complex. Except for the bimodal nature of the distribution, the fit was performed as described above. For Domain 2, $f/f_0 = 1.47$, while the f/f_0 refined for Domain 1 was 1.63. Using the former frictional ratio and the apparent *s*-value of the complex (~10.3 S), a mass of 286,204 Da was obtained for the complex. In addition, the masses obtained for GST-VCA from two different SV experiments (GST-VCA alone and GST-VCA in excess over Arp2/3) are in excellent agreement (73,682 Da and 73,899 Da, respectively).

To further evaluate the interaction between the GST-VCA dimer and Arp2/3, a different data analysis strategy was undertaken. Instead of fitting a continuous distribution to the SV data, we fitted these data assuming three or four species could be present in solution: the $(GST\text{-}VCA)_2$ dimer, Arp2/3 complex, the $(GST\text{-}VCA)_2$:Arp2/3 1:1 complex, and the 1:2 complex thereof. We used the program SEDPHAT to fit solutions of the Lamm equation for this system directly to the raw SV data, explicitly including reaction kinetics

and equilibrium association constants (Dam et al., 2005). During this fitting session, the following values were held fixed: the masses of the components, the extinction coefficients of the proteins, and the sedimentation coefficients of Arp2/3 and GST-VCA that were obtained from SV experiments with those proteins alone. Allowed to float were the sedimentation coefficient of the GST-VCA:Arp2/3 complex, the association equilibrium constant, the concentrations of the proteins, the k_{off} of the interaction, time-independent noise, and the sample meniscus. Two interaction models were considered. In the first, we fit a 1:1 interaction between the $(GST\text{-}VCA)_2$ dimer and Arp2/3 complex. The extinction coefficients of the proteins were determined from SV experiments in which only the individual components were sedimented and in which both absorbance spectrophotometry and laser interferometry were used simultaneously to follow sedimentation of the proteins. Because the signal increment that a protein exhibits in the laser interferometer is a simple multiple of its mass, these increments can be calculated and treated as *a priori* information against which the spectrophotometric extinction coefficient of the protein can be refined. The calculated and refined signal increments used for this study are presented in Table S2. The Marquardt-Levenberg minimization performed by SEDPHAT using a 1:1 interaction model converged on an excellent fit; the r.m.s. deviation of the data from the fits was 0.004215 AU, with a value for reduced chi-square (χ^2) of 1.11 (see Fig. S3). Relevant values obtained from this analysis were K_D = 84 nM (similar to that obtained by fluorescence measurements, 26 ± 7 nM, Fig. 1C), k_{off} = .002 s^{-1}, and s_{AB} (sedimentation coefficient of the complex) = 10.4 S. We also fit the data to a 1:2 model of $(GST\text{-}VCA)_2$ dimer to Arp2/3 complex (i.e. $(GST\text{-}VCA)_2$ + Arp2/3 + Arp2/3 ↔ $(GST\text{-}VCA)_2$:Arp2/3 + Arp2/3 ↔ $(GST\text{-}VCA)_2$:$(Arp2/3)_2$). This model

resulted in a fit that could not be statistically distinguished from the previous model. However, in order to obtain this result, a large, negative cooperativity between the first and second binding events (K_D (1) = 87 nM, K_D (2) = 8.7 μM) had to be modeled. Because the concentrations of the proteins do not approach K_D (2), it is impossible to distinguish between the two models. If the 1:2 model is correct, it implies that a second Arp2/3 can bind to the GST-VCA dimer only at high Arp2/3 concentrations.

Table S2. Fitted Sedimentation Velocity Parameters for GST-WASP VCA and Arp2/3 Complex.

Protein	**Interferometric signal increment** (fringes·M^{-1}·cm^{-1})*	**Refined extinction coefficient @ 280 nm** (AU·M^{-1}·cm^{-1})
GST-VCA	193,089	92,369
Arp2/3	615,516	242,602

*calculated from the mass of the protein complexes; the GST-VCA value is for the homodimer

Arp2/3 Affinity Measurements

VCA affinities for Arp2/3 complex were determined by competition against rhodamine-labeled N-WASP VCA (rVCA) (Marchand et al., 2001) or rhodamine-labeled cortactin NtA (rNtA), which bind Arp2/3 complex with K_D of 73 nM and 42 nM, respectively. Anisotropy (λ_{EX} = 552 nm, λ_{EM} = 574 nm) was measured at 22 °C on a Jovin Yvon Fluorolog-3 spectrofluorimeter equipped with automated polarizers. The dissociation constant of rVCA or rNtA for Arp2/3 complex, $K_{D,rV}$, was obtained by titrating Arp2/3 into a solution of rVCA or rNtA. In competition assays, unlabeled competitor was titrated into 10 nM rVCA plus 1 μM Arp2/3 complex or 10nM rNtA plus 200nM Arp2/3 complex in KMEI buffer. To ensure consistency, data comparing each VCA/GST-VCA pair were acquired within 48 hrs using the same Arp2/3 complex and rVCA preparations. Anisotropy data were fit using equations S1-S6 solved for $r_{observed}$ (terms in equations defined below equation S6). There are three solutions to the system of equations, only one of which will be valid for any given range of K_D, with a discontinuity occurring at $K_D = K_{D,rV}$. The binding equation was fit using the FindFit algorithm in the NonlinearRegress function of Mathematica 5.2 (Wolfram), optimizing K_D, r_{free} and r_{bound} for the best fit to the data. Errors were estimated using Monte Carlo error analysis; 1000 simulated data sets were used to estimate the 1σ confidence interval, which is the reported error.

Eq. S1: $$K_D = \frac{[Arp2/3][VCA]}{[Arp2/3:VCA]}$$

Eq. S2: $$K_{D,rV} = \frac{[Arp2/3][rVCA]}{[Arp2/3:rVCA]}$$

Eq. S3: $$[VCA]_{total} = [VCA] + [Arp2/3 : VCA]$$

Eq. S4: $$[rVCA]_{total} = [rVCA] + [Arp2/3 : rVCA]$$

Eq. S5: $$[Arp2/3]_{total} = [Arp2/3] + [Arp2/3 : VCA] + [Arp2/3 : rVCA]$$

Eq. S6: $$r_{observed} = \frac{r_{free}[rVCA] + r_{bound}[Arp2/3 : rVCA]}{[rVCA]_{total}}$$

Terms are defined as follows: $r_{observed}$ is the observed anisotropy, K_D is the affinity of the VCA competitor for Arp2/3, $K_{D,rV}$ is the affinity of the rhodamine labeled WASP VCA for Arp2/3, $[VCA]_{total}$ is the total concentration of competitor VCA in solution, [VCA] is the concentration of competitor VCA not in complex, [Arp2/3:VCA] is the concentration of VCA competitor in complex with Arp2/3, $[rVCA]_{total}$ is the total concentration of all rhodamine labeled VCA in solution, [rVCA] is the concentration of rhodamine labeled VCA not in complex, [Arp2/3:rVCA] is the concentration of rhodamine labeled VCA in complex with Arp2/3, $[Arp2/3]_{total}$ is the total concentration of Arp2/3 in solution and [Arp2/3] is the concentration of Arp2/3 not associated with VCA. For binding measurements using NtA or rNtA, concentrations of NtA or rNtA were used in lieu of VCA or rVCA concentrations in Eq. S1-S6, and the $K_{D,rV}$ used the value from rNtA instead of rVCA.

Observation of Arp2/3 Dependent FRET between VCA and NtA

Energy transfer was observed between A488-N-WASP CA and A594-NtA in the presence of Arp2/3 complex in KMEI at 22 ˚C. Fluorescence was recorded using an excitation wavelength of 470 nm (2 nm bandpass) and scanning emission wavelengths between 475 and 701 nm in 2 nm steps using a Jovin Yvon Fluorolog-3 spectrofluorimeter. The intensity of the donor (A488-N-WASP CA) changes by ~3% upon binding to Arp2/3, which complicates the comparison of bound and free A488-N-WASP CA. Instead comparisons were made between the emission spectra of Mixture 1 (500 nM A488-N-WASP CA, 500 nM A594-NtA and 500 nM Arp2/3) and the sum of the emission spectra of Mixture 2 (500 nM A488-N-WASP CA and 500 nM Arp2/3) and Mixture 3 (500 nM A594-NtA and 500 nM Arp2/3). The spectrum for each mixture is the average of at least three samples and is corrected for background scattering by subtracting the intensities of a KMEI buffer spectrum. Errors bars shown are combined standard error for three or more repeats of each spectrum. To show that the enhancement of acceptor fluorescence originates from FRET and not formation of the ternary (CA:Arp2/3:NtA) complex, photobleached A488-N-WASP CA was used in place of A488-N-WASP CA. Data were collected and errors calculated in the same fashion as above.

Isothermal Titration Calorimetry

Purified EspFu peptides and N-WASP$_C$ were dialyzed extensively against KMEI buffer plus 5 mM β-mercaptoethanol. Titrations were performed using a VP-ITC MicroCalorimeter (MicroCal) at 25°C. The baseline for each experiment was corrected and data were fit assuming a single affinity for all binding sites. Analysis of data for EspFu 2R proteins according to a two-affinity model did not yield statistical improvement in the fitting, indicating that the K_D values for the two repeats are not sufficiently different to be distinguished by this method.

Kinetic Modeling of Arp2/3 Dependent Actin Polymerization Data

Mullins and colleagues have reported a mathematical model that describes the kinetics of actin assembly by the VCA-Arp2/3 system (Zalevsky et al., 2001). To determine if the difference in Arp2/3 affinity between VCA dimers and monomers is sufficient to account for their differences in activity, we fit actin assembly data to this model (methods detailed in following section). Our hypothesis is that the affinity difference is sufficient to account for the kinetics changes. If this is correct, then only changes to the parameters describing the Arp2/3:VCA interaction will be required to fit the actin assembly data for GST-VCA and VCA. We analyzed actin assembly promoted by N-WASP VCA and GST-N-WASP VCA at a variety of actin and Arp2/3 concentrations (Fig. S6A) (Zalevsky et al., 2001). We used literature values for association and dissociation rate constants for the VCA:Arp2/3 and VCA:actin interactions (Table S3). We fit GST-N-WASP VCA data using the same rate constants, except that the VCA:Arp2/3 on- and off-rate constants were modified to reflect the 180-fold change in affinity (separately changing the on- and off- rate constants is separate fitting procedures). We fit rate constants describing mother filament association and activation of the Arp2/3 complex (described by k_{3f}, k_{3r}, and k_{4f}, see Fig. S6A) using a systematic grid search. If the values of these rate constants obtained by fitting the free VCA data agree with those obtained by fitting the GST-VCA data, then the affinity change is sufficient to account for the activity change.

Both the N-WASP VCA data and the GST-N-WASP VCA data are described well by the kinetic model (Fig. S6B, C, D, and E). We compared the fitted parameters derived from

the GST-N-WASP VCA and VCA data (the former using the modified on-rate constant to account for higher affinity). The values of k_{4f} for the two proteins are indistinguishable, e.g. 0.013μM^{-1} s^{-1} is among the best values fit for both materials (Table S4). Association of the ternary complex of VCA:actin:Arp2/3 with mother filament is also indistinguishable between N-WASP VCA and GST-N-WASP VCA. Both proteins show evidence that this step is in a pseudo equilibrium; the top fitting solutions have a wide range of values for k_{3f} and k_{3r}, but their ratio is fixed ($K_{d3} = k_{3r}/k_{3f}$) (Table S4). The two proteins have overlapping ranges of K_{d3}, with 126 nM among the best values for each. Overall, the fit parameters are not distinguishable between N-WASP VCA and GST-N-WASP VCA. Therefore, GST-N-WASP VCA is likely to activate Arp2/3 through a similar mechanism to monomeric VCA, but with higher affinity.

Table S3. Kinetic parameter symbols, values and sources.

parameter(s)	N-WASP VCA	GST-N-WASP VCA	Source
k_{1af}/k_{2bf}	5.5 $\mu M^{-1} s^{-1}$	5.5 $\mu M^{-1} s^{-1}$	(Marchand et al., 2001)
k_{1ar}/k_{2br}	3 s^{-1}	3 s^{-1}	(Marchand et al., 2001)
k_{1bf}/k_{2af}	1 $\mu M^{-1} s^{-1}$	180 $\mu M^{-1} s^{-1}$, 1 $\mu M^{-1} s^{-1}$	(Zalevsky et al., 2001) and see text
k_{1br}/k_{2ar}	0.4 s^{-1}	0.4 s^{-1}, 0.0022 s^{-1}	(Zalevsky et al., 2001) and see text
k_{3f}	fit	fit	
k_{3r}	fit	fit	
k_{4f}	fit	fit	
k_{nuc}	$1.6*10^{-9}$ $\mu M^{-3} s^{-1}$	$1.6*10^{-9}$ $\mu M^{-3} s^{-1}$	Determined from actin only data
$k_{belongf}$	10 $\mu M^{-1} s^{-1}$	10 $\mu M^{-1} s^{-1}$	(Fujiwara et al., 2007)
$k_{belongr}$	1 s^{-1}	1 s^{-1}	(Fujiwara et al., 2007)
$k_{pelongf}$	1 $\mu M^{-1} s^{-1}$	1 $\mu M^{-1} s^{-1}$	(Fujiwara et al., 2007)
$k_{pelongr}$	0.1 s^{-1}	0.1 s^{-1}	(Fujiwara et al., 2007)

Table S4. Fitting Results using Kinetic Model.

	$K_{d3} = k_{3r}/k_{3f}$*	lower limit for k_{3f}	k_{4f} range *	best sum of $(\text{residuals})^2$
N-WASP VCA	126 nM	25 $\mu M^{-1} s^{-1}$	0.013 $\mu M^{-1} s^{-1}$	65.8 μM^2
GST-N-WASP VCA change k_{1bf} and k_{2af}	80-126 nM	10 $\mu M^{-1} s^{-1}$	0.010-0.013 $\mu M^{-1} s^{-1}$	39.9 μM^2
GST-N-WASP VCA change k_{1br} and k_{2ar}	100-158 nM	10 $\mu M^{-1} s^{-1}$	0.025-0.032 $\mu M^{-1} s^{-1}$	69.2 μM^2

* range of values considered were those up to best sum of square of residual + 5%.

Methods for global fitting of kinetic data

Actin assembly kinetics were fit by searching for a set of rate constants which minimized the difference between the data and the filamentous actin kinetic progress curves predicted by the kinetic model described below. The kinetic model combined with a trial set of rate constants and a set of initial concentrations for all species (dictated by the concentrations used in a given experiment), defines a system of differential equations with a boundary value. This system can be numerically integrated to yield a kinetic progress curve, here using the NDSolve function in Mathematica 5.2 (Wolfram). To fit a set of data (eg. the free VCA titrations), more than 10,000 trial rate constant sets were generated. Each trial set used the fixed values described in Table S3, and a set of values of k_{3f}, k_{3r}, and k_{4f} that were drawn from a list of values that systematically sampled a space containing at least a 30-fold range of each parameter, in geometric steps of ~1.25. These rate constants were then applied to a set of initial conditions describing the actin and Arp2/3 titrations, the resulting series of boundary value problems were integrated to generate a series of predicted kinetics. A global sum of squares of residuals was calculated by comparisons between appropriate predicted curves and data. To allow this calculation, the raw fluorescence intensities from actin assembly assays were converted to filamentous actin (fActin) units by assuming the change in fluorescence intensity varied linearly with fActin, and that total fActin produced at maximum intensity was (total actin)-(actin critical concentration). The rate constant set giving the lowest global sum of squares of residuals was considered the best fit, and the parameter ranges reported in Table S4 considered the best fit and fits up with up to a 5% increase in global sum of squares of residuals.

The kinetic mechanism of Arp2/3 dependent actin assembly (Fig. S6A) (Zalevsky et al., 2001) was converted the following set of rate laws (Eqs. S7-S16).

Eq. S7
$$[NPF]'(t) = -k_{1af}[NPF](t)[gActin](t) + k_{1ar}[NPF:gActin](t) \\ -k_{1bf}[NPF](t)[Arp2/3](t) + k_{1br}[NPF:Arp2/3](t)$$

Eq. S8
$$[Arp2/3]'(t) = -k_{1bf}[NPF](t)[Arp2/3](t) + k_{1br}[NPF:Arp2/3](t) \\ -k_{2af}[NPF:gActin](t)[Arp2/3](t) + k_{2ar}[NPF:Arp2/3:gActin](t)$$

Eq. S9
$$[gActin]'(t) = -k_{1af}[NPF](t)[gActin](t) + k_{1ar}[NPF:gActin](t) \\ -k_{2bf}[NPF:Arp2/3](t)[gActin](t) + k_{2br}[NPF:Arp2/3:gActin](t) \\ -nk_{nuc}[gActin](t)^n - k_{belongf}[bEnd](t)[gActin](t) - k_{pelongf}[pEnd](t)[gActin](t) \\ +k_{belongr}[bEnd](t) + k_{pelongr}[pEnd](t)$$

Eq. S10
$$[fActin]'(t) = -k_{3f}[NPF:Arp2/3:gActin](t)[fActin](t) \\ +k_{3r}[fActin:NPF:Arp2/3:gActin](t) + 2k_{4f}[fActin:NPF:Arp2/3:gActin](t) \\ +nk_{nuc}[gActin](t)^n + k_{belongf}[bEnds](t)[gActin](t) + k_{pelongf}[pEnd](t)[gActin](t) \\ -k_{belongr}[bEnd](t) - k_{pelongr}[pEnd](t)$$

Eq. S11
$$[NPF:gActin]'(t) = k_{1af}[NPF](t)[gActin](t) - k_{1ar}[NPF:gActin](t) \\ -k_{2af}[NPF:gActin](t)[Arp2/3](t) + k_{2ar}[NPF:Arp2/3:gActin](t)$$

Eq. S12
$$[NPF:Arp2/3]'(t) = k_{1bf}[NPF](t)[Arp2/3](t) - k_{1br}[NPF:Arp2/3](t) \\ -k_{2bf}[NPF:Arp2/3](t)[gActin](t) + k_{2br}[NPF:Arp2/3:gActin](t)$$

Eq. S13
$$[NPF:Arp2/3:gActin]'(t) = k_{2af}[NPF:gActin](t)[Arp2/3](t) \\ -k_{2ar}[NPF:Arp2/3:gActin](t) + k_{2bf}[NPF:Arp2/3](t)[gActin](t) \\ -k_{2br}[NPF:Arp2/3:gActin](t) - k_{3f}[NPF:Arp2/3:gActin](t)[fActin](t) \\ +k_{3r}[fActin:NPF:Arp2/3:gActin](t)$$

Eq. S14 $$[fActin:NPF:Arp2/3:gActin]'(t) = k_{3f}[NPF:Arp2/3:gActin](t)[fActin](t) - k_{3r}[fActin:NPF:Arp2/3:gActin](t) - k_{4f}[fActin:NPF:Arp2/3:gActin](t)$$

Eq. S15 $$[bEnd]'(t) = k_{4f}[fActin:NPF:Arp2/3:gActin](t) + k_{nuc}[gActin](t)^n$$

Eq. S16 $$[pEnd]'(t) = k_{nuc}[gActin](t)^n$$

Quantities in square brackets "[]" represent the concentration of the named species at a given time 't', eg. the concentration of Arp2/3 at a given time is represented by [Arp2/3](t). Primed quantities (eg. [NPF]'(t)) are the rates of change of the concentrations. NPF is nucleation promoting factor, representing either N-WASP VCA or (GST-N-WASP VCA)$_2$. gActin and fActin represent soluble globular actin and filamentous actin (in monomer units), respectively. In addition to total fActin, filament barbed ends, [bEnd](t), and filament pointed ends, [pEnd](t), are tracked to give a reasonable description of the bulk filament behavior. Higher order assemblies are indicated by names joined by a colon (eg. [NPF:Arp2/3:gActin] is the concentration of the ternary complex, Arp2/3 bound to NPF and gActin). Rate constants are represented by k_x where 'x' indicates the associated step in the mechanism. Most rate constants are shown in Fig. S6A. Rate constants for actin assembly (not shown in Fig. S6A) are: k_{nuc} (combined *de novo* nucleation rate constant), *n* (the reaction order of *de novo* nucleation, the smallest stable filament here), $k_{belongf}$ (barbed end elongation forward rate constant), $k_{belongr}$ (barbed end elongation reverse rate constant), $k_{pelongf}$ (pointed end elongation forward rate constant) and $k_{pelongr}$ (pointed end elongation reverse rate constant). The model does not attempt to account for: fActin ATP hydrolysis or phosphate release,

which have small effects on pyrene intensity, branch disassembly, filament fission, and cooperative assembly of the ternary complex. Additionally, all VCA materials were assumed to have one actin-binding site. This is reasonable given that under our conditions, actin association with the VCA material will be nearly saturated (initial actin concentration is greater than or equal to 10-fold the K_D for actin, VCA association, > 4 μM vs. 0.4 μM). Most parameters are fixed to literature values (Table S3). The value of k_{nuc}, $1.6*10^{-9}$ μM^{-3} s^{-1}, was determined from fitting of *de novo* actin nucleation data (not shown).

Equilibrium Modeling of WASP/Dimerizer/Arp2/3 Equilibria

We modeled the concentration of active Arp2/3 complex ($[Arp2/3]_{Bound}$, Eq. S24) according to equations S17-S23, which were solved iteratively by converting to a series of rate laws that were integrated over time at least ten-fold beyond any observable change. Integration was accomplished using the NDSolve function in Mathematica 5.2. To model the effects of dimerizing constitutively active WASP, equations S17-S23 were used, with $K_{D1} = K_{D2} = 1$ μM. To model the enhanced affinity of dimeric ligands toward Arp2/3, $K_{D3} = 0.01$ μM, except where noted. Monomeric ligands (D) were used to simulate the back titration and titration of non-dimeric ligands. When modeling dimerizers (DD) whose binding is coincident with activation of autoinhibited WASP (e.g. EspFu), we omitted equation S19 (i.e. only dimerizer-bound WASP was assumed to bind Arp2/3 complex).

Equation S17: $\frac{1}{2}K_D = \frac{[WASP][DD]}{[WASP:DD]}$

Equation S18: $2K_D = \frac{[WASP][WASP:DD]}{[WASP:DD:WASP]}$

Equation S19: $K_{D1} = \frac{[WASP][Arp2/3]}{[Arp2/3:WASP]}$

Equation S20: $K_{D2} = \frac{[Arp2/3][WASP:DD]}{[Arp2/3:WASP:DD]}$

Equation S21: $K_{D3} = \frac{[Arp2/3][WASP:DD:WASP]}{[Arp2/3:WASP:DD:WASP]}$

Equation S22: $K_D = \frac{[WASP][D]}{[WASP:D]}$

Equation S23: $K_{D2} = \frac{[Arp2/3][WASP:D]}{[Arp2/3:WASP:D]}$

Equation S24:

$$[Arp2/3]_{Bound} = [Arp2/3:WASP] + [Arp2/3:WASP:DD] + [Arp2/3:WASP:DD:WASP] + [Arp2/3:WASP:D]$$

Lipid Cosedimentation Experiments

Cosedimentation studies were performed by reconstituting vesicles in 100 mM KCl, 10 mM imidazole pH 7.0, 1 mM $MgCl_2$, 1 mM EGTA, and 100 mM Sucrose and processing into vesicles as described above. Protein and lipids were mixed to 200 nM N-$WASP_B$ with 2 μM PIP_2 in carrier lipid, or carrier lipid to match the 20 % PIP_2 conditions, or no lipid. Final volume was 150 μL. Solutions were mixed such that final buffer conditions were KMEI + 10mM sucrose. Mixtures were incubated for 10 minutes at 22˚C, and then centrifuged at 65,000 rpm in a TLA-100.3 rotor (175,000 g) (Beckman) for one hour at 22˚C. Supernatants (145 μL) were removed within five minutes of the end of the spin, and pellets were resuspended in KMEI following ten minutes of soaking. The fraction of protein bound was estimated from silver stained SDS-PAGE band intensities, integrating the bands using NIH ImageJ. Using a fixed area, the average of background intensity immediately above and below the band was used to calculate the background intensity, such that integrated band intensity could be converted to an apparent optical density. While silver stain is not frequently used for quantification purposes, we found that our protocol provided linear estimates of protein concentrations between 40 nM and 250 nM (Fig. S13A). Thus, our quantification should be reasonable with the exception of the lowest intensity bands (e.g. the pellet of the no lipid sample, Fig. S13B). Additionally, the intensities of most of the quantified bands are quite similar, implying that any actual nonlinearities in the silver stain signal will have minimal impact on the results.

Increased Complexity of the WASP Allosteric Switch Afforded by Hierarchical Regulation

The hierarchical model for regulation of WASP/WAVE proteins provides a second layer of regulation (dimerization/oligomerization) that increases the complexity afforded by the WASP allosteric switch. For example, our modeling predicts that changes in the affinity of dimerizer for WASP can alter qualitative behavior in a titration (Fig. 3C); higher affinity produces a sharper peak in activity, which occurs at lower dimerizer concentration. This is borne out in comparison of the PACSIN2, EspFu 2R and EspFu $2R_C$ titrations (Figs. 4D, 4A and S11). The response to multi-SH3 ligands will vary significantly between proteins. Different SH3 domains will have distinct specificities for the numerous proline rich motifs in WASP proteins. For a given multi-SH3 ligand, these specificities will determine the balance between inter-WASP and intra-WASP contacts, where only the former result in oligomerization.

These distinct specificities will also determine the degree to which different SH3 ligands can bind to preassembled WASP complexes. The binding of different multi-SH3 ligands into such multi-WASP complexes will occur with positive cooperativity. For example, if a pair of WASP molecules are dimerized by a low affinity SH3 domain that contacts only one site, the complex will be greatly stabilized by the binding of a second low affinity dimerizer that recognizes a different site. This will allow hyperactivation in response to much lower ligand concentrations. This idea also generalizes to non-SH3 secondary ligands, including PIP_2 or Cdc42 rich regions of membranes. It is especially interesting to consider the effects of SH3 containing proteins that also bind membranes (eg. F-BAR

proteins such as PACSIN, SNX9 or CIP4). For these systems, assembly formation and membrane binding should be thermodynamically coupled. In other words, larger complexes, which contain more membrane interaction motifs (e.g. basic regions, GBDs, F-BAR dimers), should bind membranes more tightly. Reciprocally, membrane associated WASP molecules must be more readily associated into assemblies. The combination of allostery and dimerization/oligomerization enables precise tuning of actin assembly activities, depending on the nature and concentrations of WASP ligands activated in a particular time and place during a biological process.

Probabilistic Enhancement of WASP Protein Activity

Increasing number of repeats in EspFu proteins.

At equal total repeat concentrations, a five repeat EspFu construct is more active than a two repeat construct (Fig. 5A). This difference can be explained through a probabilistic argument. We derived a simple relationship between n, the number of repeats, P_m, the probability of a given repeat being engaged with an active WASP molecule, and P_d, the probability that a given EspFu molecule will be bound to two or more active WASP molecules. Since each EspFu repeat binds WASP independently (see main text), the value of P_m is dictated solely by the K_D of the interaction and the concentrations of total repeats (R_T) and WASP in solution. That is, at identical WASP and total repeat concentrations, the same number of WASP proteins will be activated (P_m will be constant), regardless of the size of n. Initially, we considered a construct with two identical repeats, which has the following possible combinations:

First Repeat	Second Repeat	Probability
Empty	Empty	$(1- P_m)(1- P_m)$
Bound	Empty	$P_m(1- P_m)$
Empty	Bound	$(1- P_m)P_m$
Bound	Bound	$P_m P_m$

Thus, the probability of one repeat being bound is $2P_m(1- P_m)$ and the probability of both repeats being bound is P_m^2. It follows from considering the possible combinations for a general case that P_d is given by Eq. S25 (Devore, 2000).

Equation S25: $P_d = \sum_{k=2}^{n} \frac{n!}{k!(n-k)!} {P_m}^k (1-P_m)^{n-k}$

The concentration of EspFu molecules bound to two or more WASP proteins (which equals the concentration of WASP dimers/oligomers, [$WASP_{2+}$]) is then given by Eq. S26.

Equation S26: $[WASP_{2+}] = [EspFu] P_d$

To isolate the effects of n, different EspFu constructs must be compared at the same R_T, where [EspFu] = R_T/n (maintaining constant [EspFu] would vary R_T, and thus the concentration of active WASP, in addition to n). It follows then that the concentration of WASP dimer/oligomer assembled on EspFu molecules of repeat number n, at fixed R_T is given by Eq. S27.

Equation S27: $[WASP_{2+}] = \frac{R_T}{n} \sum_{k=2}^{n} \frac{n!}{k!(n-k)!} {P_m}^k (1-P_m)^{n-k}$

Eq. S27 can be simplified to an intuitively meaningful form by considering a situation where P_m is small, and thus $(1\text{-}P_m)^{n-k}$ is approximately 1. In this regime, the right most term is dropped and ${P_m}^2 >> {P_m}^3 >> \ldots >> {P_m}^n$. Where the later is true we can reasonably consider only the $k = 2$ term and the equation reduces to:

Equation S28:

$$[WASP_{2+}] \approx \frac{R_T}{n}\left(\frac{n!}{2(n-2)!}P_m{}^2\right)$$
$$\approx \frac{R_T P_m{}^2}{2}(n-1)$$

Thus, the concentration of dimeric/oligomeric WASP assemblies will scale as (n-1), such that at constant R_T and constant WASP concentration, 2R, 3R and 5R constructs produce 1-, 2- and 4-fold the concentrations of $WASP_{2+}$ species, respectively. Although the approximation $(1\text{-}P_m)^{n-k} \sim 1$ is only correct for very small values of P_m, higher values of P_m will still give the same relative order of activity (activity of an n repeat construct > activity of (n-1) repeat construct). For example, when P_m = 0.2, 2R, 3R and 5R constructs produce 1-, 1.7- and 2.6-fold the concentrations of $WASP_{2+}$ species, respectively.

Activation through control of size of WASP clusters

As described in the discussion, WASP proteins often function within large complexes that are predicted to contain multiple WASP molecules. Assembly of these complexes appears to increase activity toward Arp2/3 complex. This effect can be understood probabilistically, through an argument analogous to the one above regarding increasing repeat numbers in EspFu constructs. Mathematically, the two are identical; with a slight redefinition of terms, equation S25 describes the probability that arbitrarily assembled clusters of WASP molecules (e.g. through SH3 proteins or PIP_2 association) will contain two or more active WASPs. In this case, P_m is the probability that any given WASP molecule will be open (VCA released from GBD), n is the size of the cluster (number of total WASP molecules within it), and P_d is the probability that the complex will contain two or more open WASP molecules (and thus stimulate Arp2/3 complex with high

potency). The plots in Fig. 5B result from choosing values for P_d and n and solving equation S25 for $0 < P_m < 1$. As can be seen in Fig. 5B, P_d, and thus the activity of the clusters toward Arp2/3 complex, can be raised by either increasing the fraction of WASP molecules that are open and active (increasing P_m), or by increasing the size of the cluster (increasing n). Thus, assembly of WASP clusters is, in and of itself a means of enhancing Arp2/3-mediated actin assembly. Alternatively, larger clusters require less allosteric input (lower P_m) than smaller clusters to achieve similar activity, and clustering potentiates allosteric stimulation. Many activators (e.g. high density, membrane bound Cdc42-GTP) will effectively increase P_m and n simultaneously.

SUPPLEMENTAL FIGURES

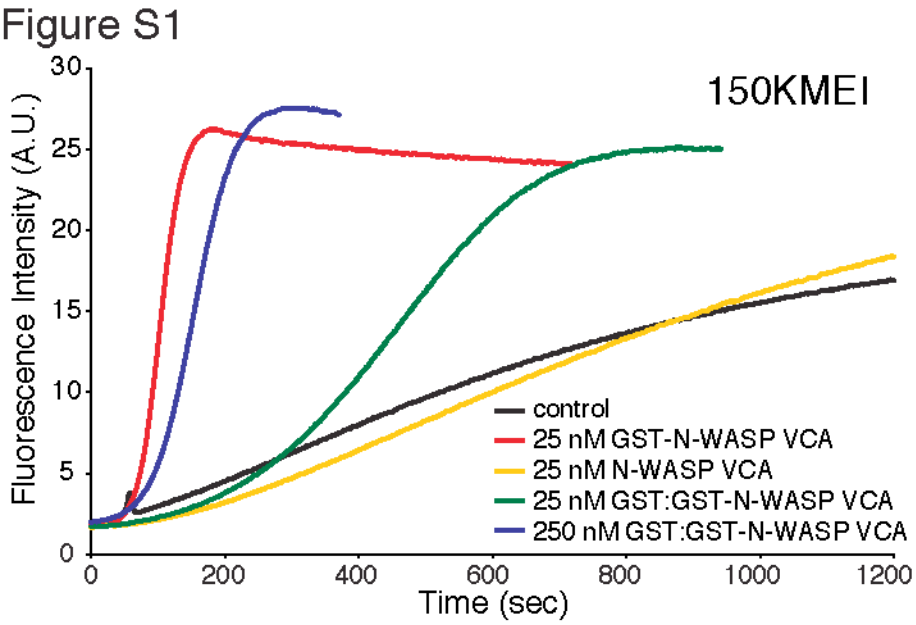

Figure S1. GST:GST-N-WASP VCA is less active than GST-N-WASP VCA.

Pyrene-actin fluorescence measured during Arp2/3-mediated actin assembly (black) in the presence of 25 nM GST-N-WASP VCA homodimer (red), 25 nM N-WASP VCA (yellow) or GST:GST-N-WASP VCA heterodimer (25 nM green, 250 nM blue). Assays performed in 150KMEI buffer. The residual activity of the GST:GST-N-WASP VCA relative to VCA is likely due to formation of $(GST\text{-}N\text{-}WASP)_2$ homodimer during handling (see Supplementary Methods).

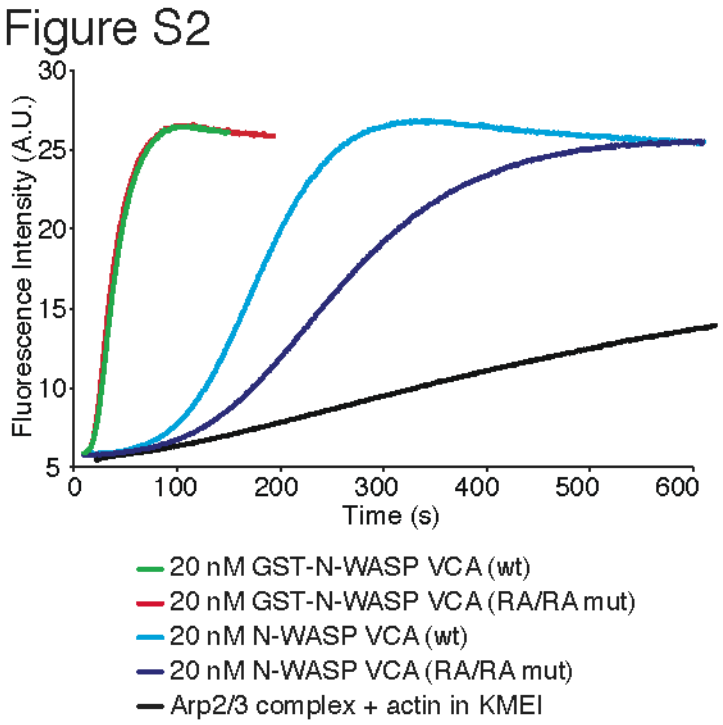

Figure S2. GST-VCA enhancement in barbed end capture deficient mutants.

Pyrene fluorescence measured during assembly of actin by Arp2/3 complex (black) plus the indicated components. 20 nM N-WASP VCA wild type (cyan), 20 nM GST-N-WASP VCA wild type (green), 20 nM N-WASP VCA RA/RA mutant (blue) and 20 nM GST-N-WASP VCA RA/RA mutant (red) in KMEI.

Figure S3

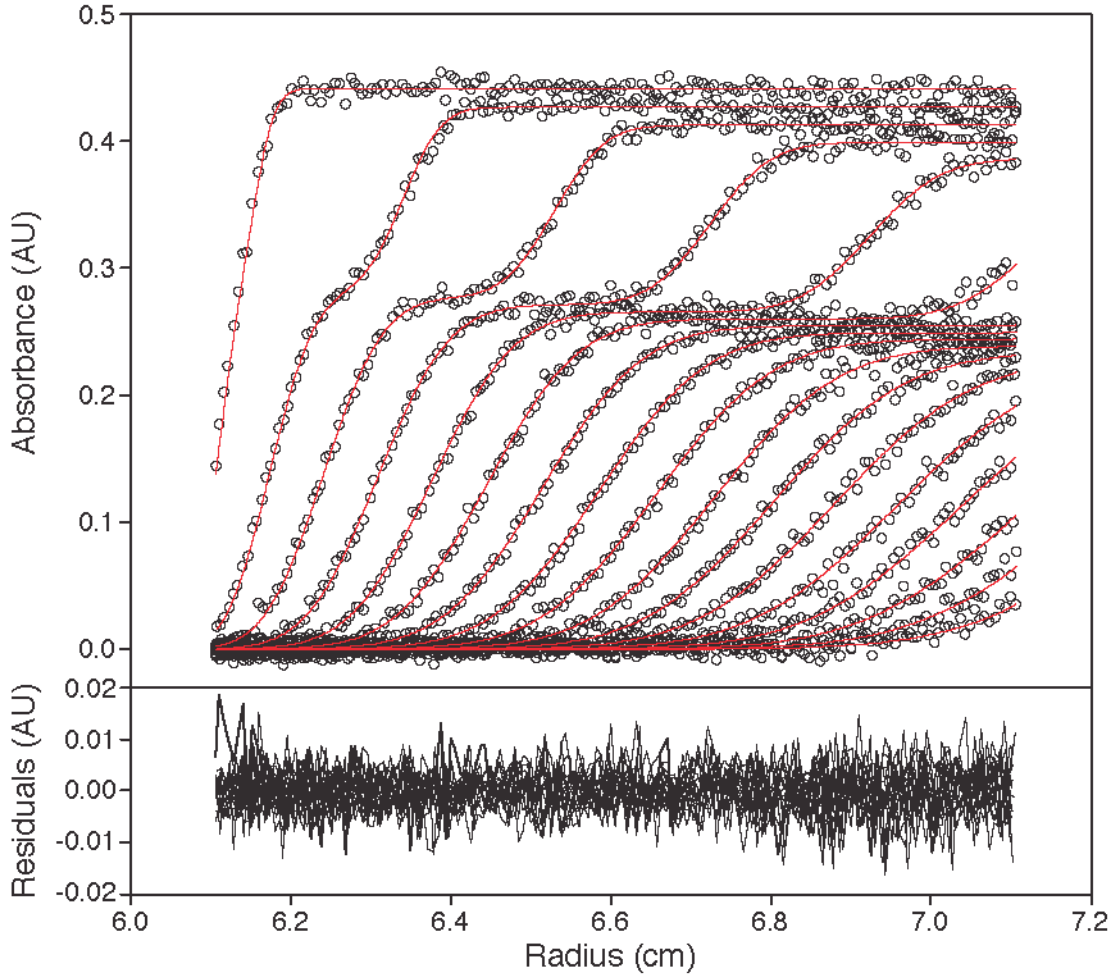

Figure S3. Solutions of the Lamm Equation Fit to the Sedimentation Velocity Ultracentrifugation Data.

Upper panel shows raw data (circles) and best fit of the Lamm equation (red lines). For clarity, only every third data point of every third scan are shown. Data were fit using solutions to the Lamm equation that take the equilibrium association constant and the kinetics of the $(GST\text{-}VCA)_2$ + Arp2/3 ↔ $(GST\text{-}VCA)_2$:Arp2/3 interaction into account. Bottom panel shows residuals of the fit.

Figure S4

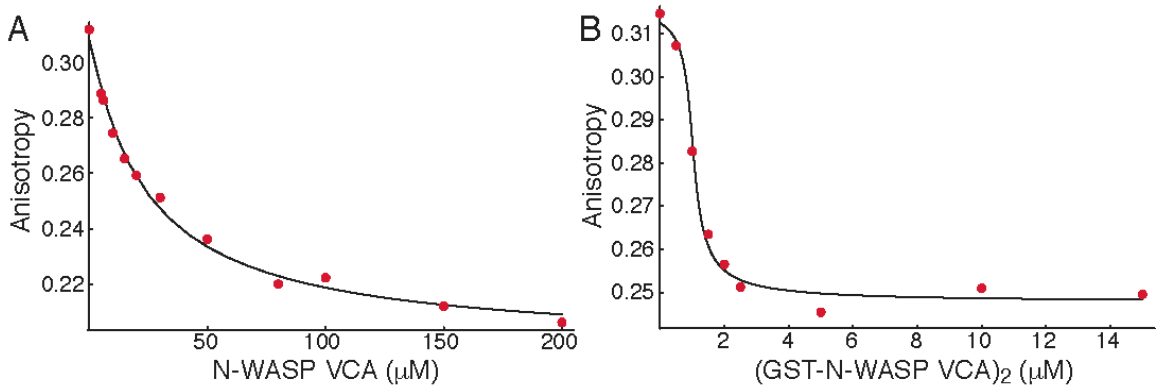

Figure S4. VCA Affinity Determined by Competition Binding.

Fluorescence anisotropy of 10 nM rhodamine N-WASP VCA in the presence of 1 μM Arp2/3 complex and the indicated competitor VCA concentrations: (A) N-WASP VCA, (B) GST-N-WASP VCA. Black curves show the best fit to equations describing competitive binding (see Methods). Data and fits for WASP VCA, GST-WASP VCA, WAVE1 VCA and GST-WAVE1 VCA are similar (not shown).

Figure S5

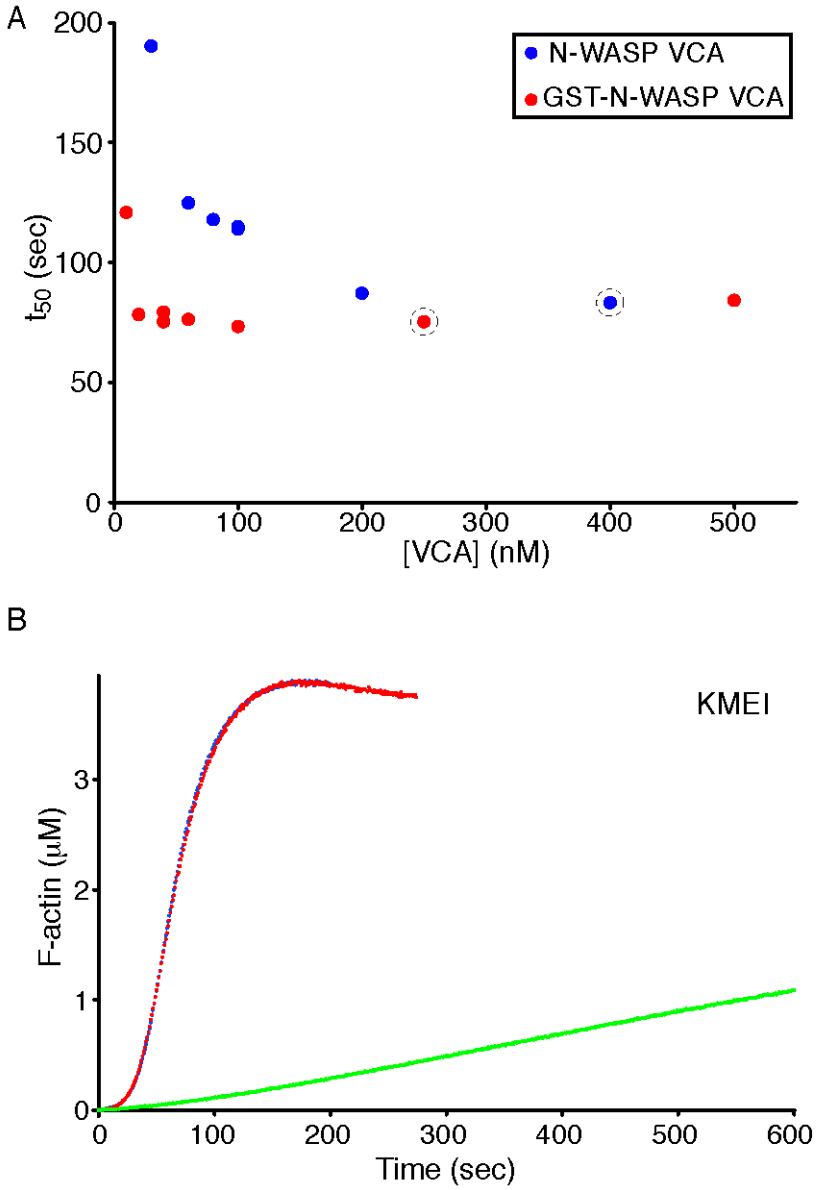

Figure S5. Saturating Activity of N-WASP VCA and GST-N-WASP VCA.

(A) Activity of N-WASP VCA (blue points) or GST-N-WASP VCA (red points) in Arp2/3-mediated actin assembly assays. The actin assembly curves shown in (B) correspond to the circled points in (A) with the same color. Green curve is *de novo* assembly of 4 μM actin. Assays performed in KMEI.

Figure S6

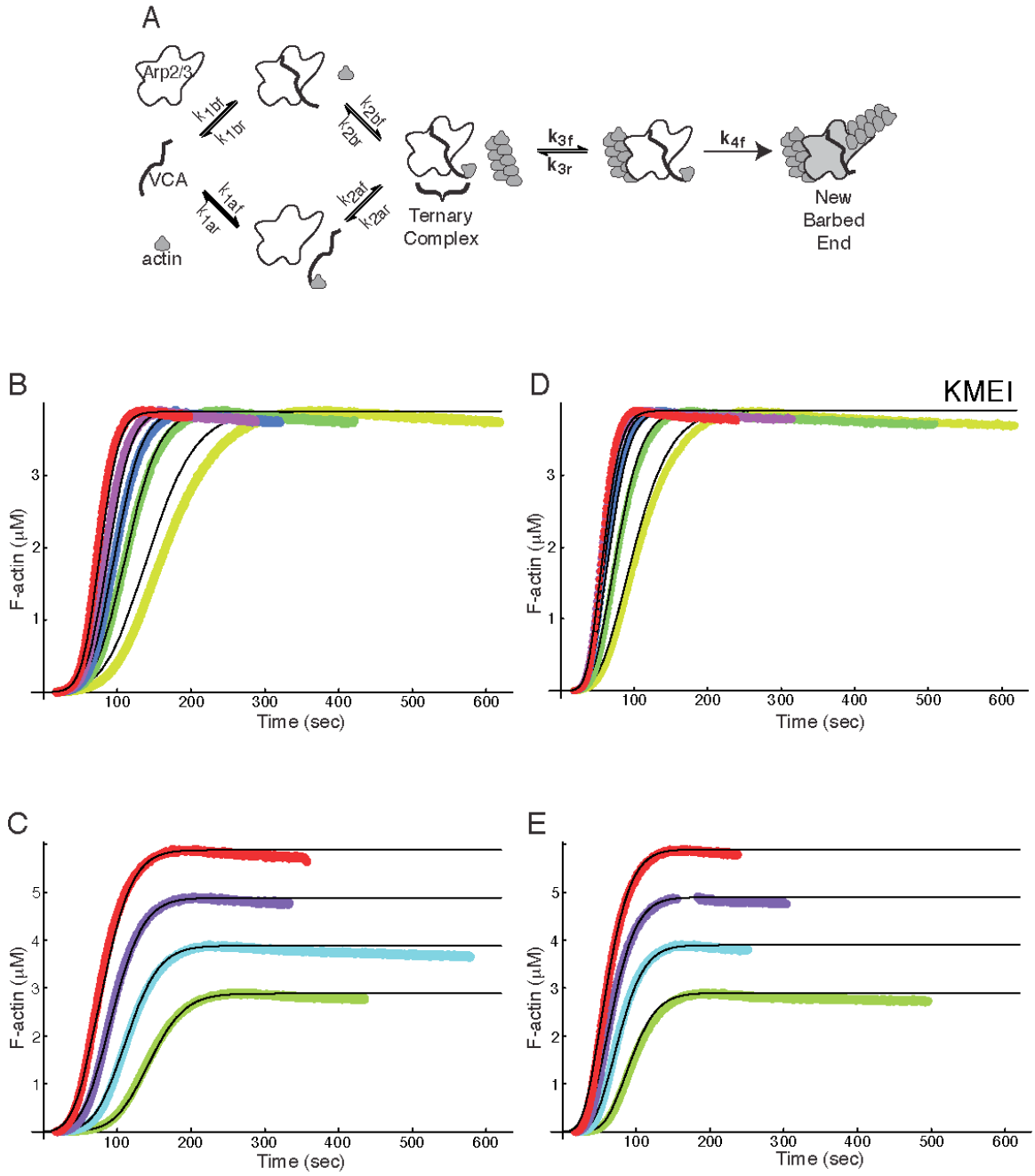
A
Arp2/3
VCA
actin
k-1bf
k-1br
k2bf
k2br
k1af
k1ar
k2af
k2ar
Ternary Complex
k3f
k3r
k4f
New Barbed End
B
D
KMEI
C
E
F-actin (μM)
Time (sec)
100
200
300
400
500
600
1
2
3
4
5

Figure S6. Kinetic Modeling of Actin Assembly.

Kinetic modeling of actin assembly assays. (A) Cartoon illustrates a previously reported mechanism for Arp2/3 dependent actin assembly. Rate constants labeled in bold were varied during fitting. (B)-(E) Colored curves show time-courses of filamentous actin assembly at a range of actin and Arp2/3 concentrations for monomeric N-WASP VCA and dimeric GST-N-WASP VCA. Black lines are best fit curves from kinetic modeling based on the mechanism shown in (A). (B), (D) Arp2/3 complex titrations were performed with 4 μM actin and 100 nM N-WASP VCA (B) or 40 nM GST-N-WASP VCA (D) at Arp2/3 concentrations of 5 nM (yellow), 10 nM (green), 15 nM (blue), 20 nM (purple) and 30 nM (red). (C), (E) Actin titrations were performed at 10 nM Arp2/3 and 100 nM N-WASP VCA (C) or 40nM GST-N-WASP VCA (E) at actin concentrations of 3 μM (green), 4 μM (cyan), 5 μM (purple) and 6 μM (red). Assays performed in KMEI.

Figure S7

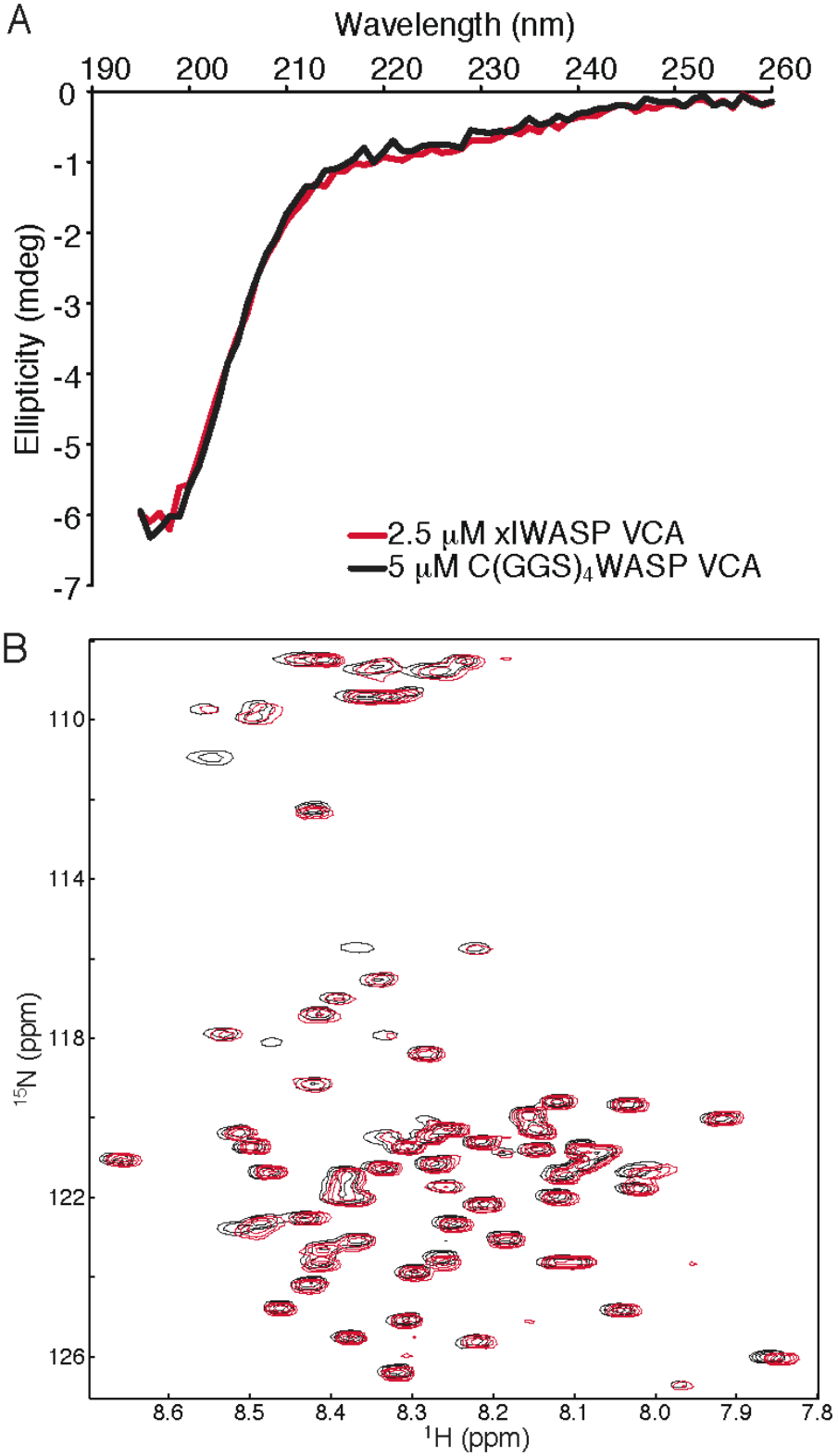
A
Wavelength (nm)
190
200
210
220
230
240
250
260
0
-1
-2
-3
-4
-5
-6
-7
Ellipticity (mdeg)
2.5 μM xlWASP VCA
5 μM C(GGS)4WASP VCA
B
110
114
118
122
126
15N (ppm)
8.6
8.5
8.4
8.3
8.2
8.1
8.0
7.9
7.8
1H (ppm)

Figure S7. Dimeric VCA is structurally indistinguishable from monomeric VCA.

(A) Far UV CD spectra of 2.5 μM dimeric xlWASP VCA (dimer units, red curve) and 5 μM monomeric $C(GGS)_4$WASP VCA (monomer units, black curve) in 5 mM HEPES pH 7.0, 50 mM KCl, 1 mM $MgCl_2$. The two curves are essentially indistinguishable and both show the characteristic minima near 196 nm indicative of random coil structure. Spectra acquired at 25˚C using an AVIV 62DS spectrometer and a 1 mm pathlength. (B). Overlaid $^{1}H/^{15}N$ HSQC spectra of xlWASP VCA (80 μM, red curve) and $C(GGS)_4$WASP VCA (19 μM, black curve) in 10 mM sodium phosphate pH 6.5, 50 mM KCl, 1 mM EGTA, 1 mm DTT recorded at 25˚C. Spectra are nearly indistinguishable and show small chemical shift dispersion, indicative of unfolded structure. Spectra acquired on a Varian Inova 600 MHz spectrometer equipped with a cold probe.

Figure S8

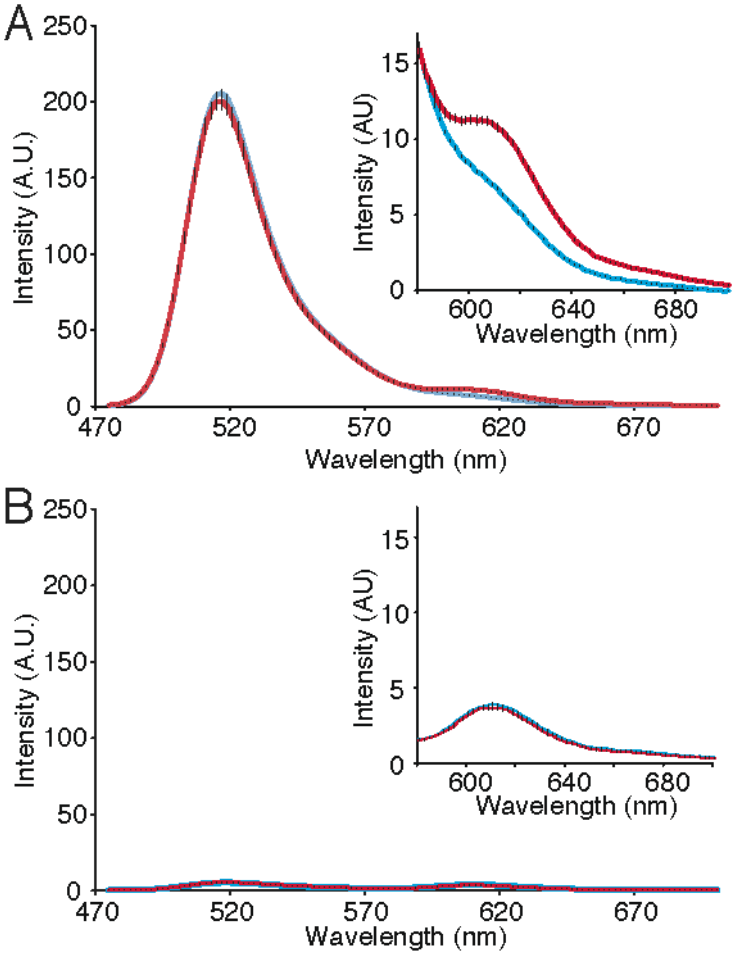
A
B
Intensity (A.U.)
Wavelength (nm)
Intensity (AU)
Wavelength (nm)
0
50
100
150
200
250
470
520
570
620
670
5
10
15
600
640
680

Figure S8. Arp2/3-induced FRET between fluorescent N-WASP and cortactin peptides.

An N-WASP CA peptide (residues 465-505) was labeled with Alexa488 (A488-N-WASP CA) and the cortactin NtA peptide was labeled with Alexa594 (A594-NtA). (A) Red curve shows the fluorescence emission spectrum (λ_{ex} = 470 nm) of a mixture of 500 nM each of A488-N-WASP CA, A594-NtA and Arp2/3 complex. Blue curve is the summation of spectra of 500 nM A488-N-WASP CA + 500 nM Arp2/3 complex and of 500 nM A594-NtA + 500 nM Arp2/3 complex. FRET between the two fluorophores is indicated in the red curve by the enhanced Alexa594 (acceptor) emission peak at 610 nm relative to the cyan curve. Inset shows an expanded view of the increased acceptor emission. A mixture of A488-N-WASP CA and A594-NtA without Arp2/3 do not show evidence of enhanced acceptor emission, however, additive spectra were used here to account for intensity changes (~5%) in A488-N-WASP CA fluorescence upon binding to Arp2/3. (B) Fluorescence emission spectra as in panel A, but acquired with photobleached (97%) A488-N-WASP CA. The enhanced A594-NtA (acceptor) peak is absent when A488-N-WASP CA is photobleached, indicating the enhancement observed on panel A is due to FRET between the fluorophores. Panels (A) and (B) and their respective insets have the same units and can be compared. Black vertical bars are a combined 1σ standard error estimatefor at least three repeats of each spectrum. An excitation wavelength of 470 nm was used to reduce the direct excitation of Alexa594, while allowing efficient excitation of Alexa488.

Figure S9

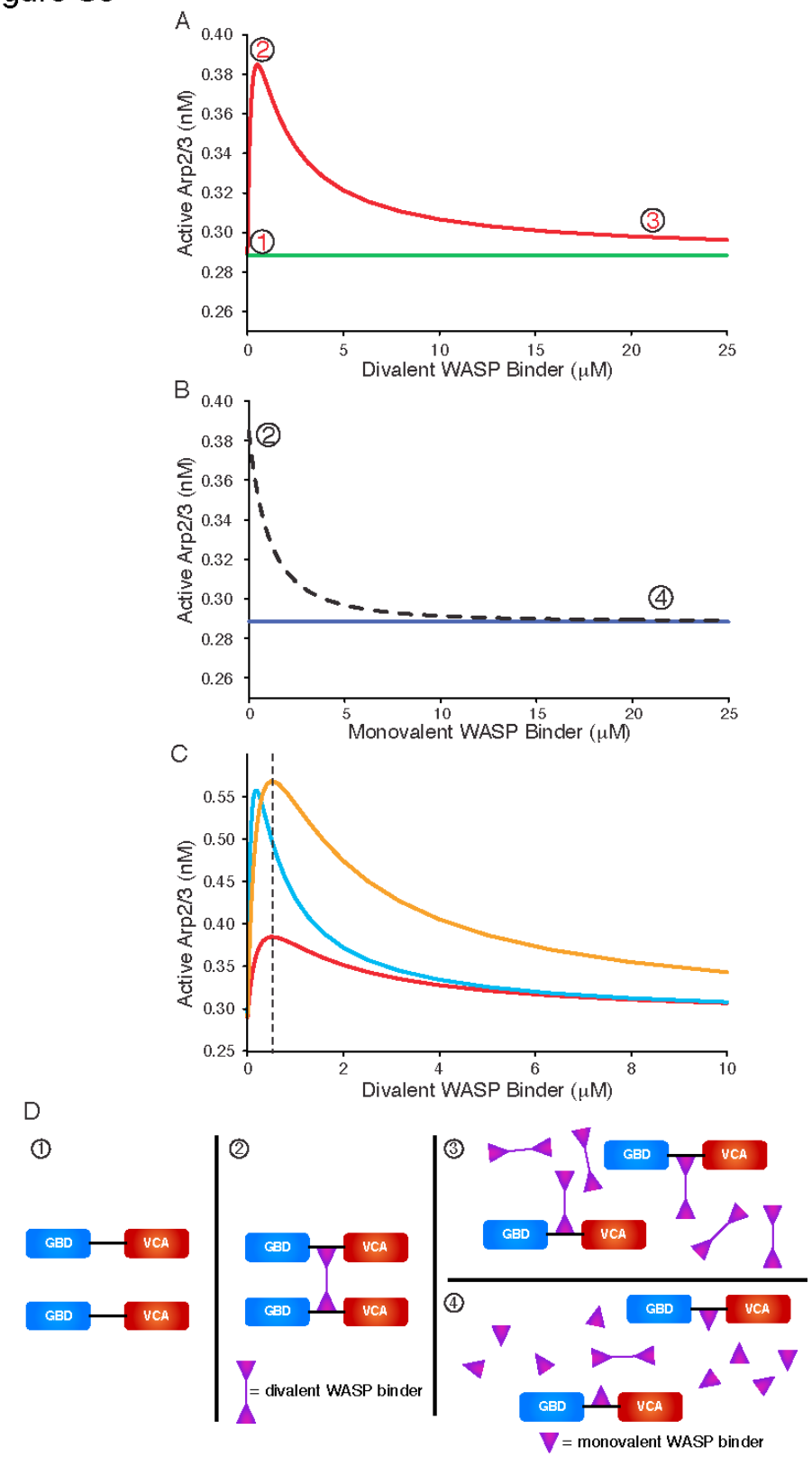
A
Active Arp2/3 (nM)
Divalent WASP Binder (μM)
B
Active Arp2/3 (nM)
Monovalent WASP Binder (μM)
C
Active Arp2/3 (nM)
Divalent WASP Binder (μM)
D
GBD
VCA
= divalent WASP binder
= monovalent WASP binder

Figure S9. Modeling Predicts Unusual Behavior in SH3 Dimer Titrations.

The concentration of active Arp2/3 complex was modeled as a function of SH3 proteins with different properties. WASP proteins are treated here as constitutively active (WASP*) and containing only a single SH3 binding site. (A) Simulated titrations of SH3 monomer (green) or SH3 dimer (red) into WASP* plus Arp2/3 complex. Blue line indicates activity of VCA (obscured by green line). (B) Simulated titration of SH3 monomer (dotted black) into WASP* hyperactivated by 500 nM $(SH3)_2$ (maximum activity in A). Blue line indicates activity of VCA. (C) Simulated titrations of different dimeric SH3 proteins into N-WASP plus Arp2/3 complex. Titration from (A) is red (note change of X- and Y-scales). Blue curve models a $(SH3)_2$ dimer with 3-fold tighter affinity for WASP than in (A), orange curve models a $(SH3)_2$:$(WASP)_2$ complex with three-fold tighter affinity for Arp2/3 than in (A). Modeling based on 25 nM WASP*, 10 nM Arp2/3 complex throughout, and the following affinities in (A) and (B)—SH3:WASP*, 1 μM; WASP*:Arp2/3, 1 μM; $(SH3)_2$:$(WASP)_2$:Arp2/3, 10 nM. (D) Cartoons illustrating the relevant species during the SH3 titrations. Circled numbers correspond to the states shown in (A) and (B).

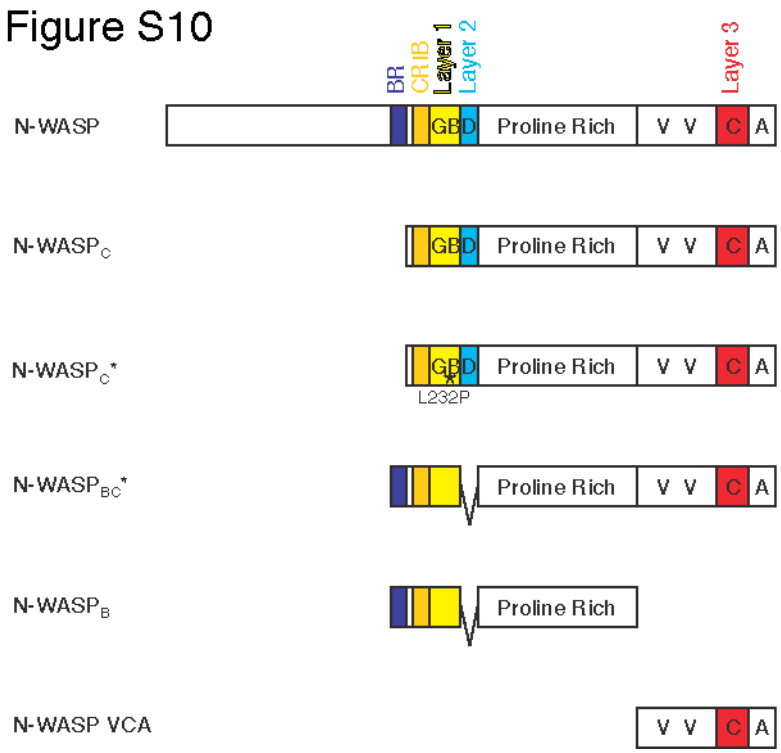

Figure S10. N-WASP Constructs Used in This Work.

BR = basic region; CRIB = Cdc42/Rac interactive binding domain; GBD = GTPase binding domain; V = verprolin homology region; C = central hydrophobic region; A = acidic region. Layers 1, 2 and 3 refer to the different elements of the autoinhibited GBD-VCA three-dimensional structure (Kim et al., 2000). L232P indicates the constitutively activating N-WASP mutation (Devriendt et al., 2001).

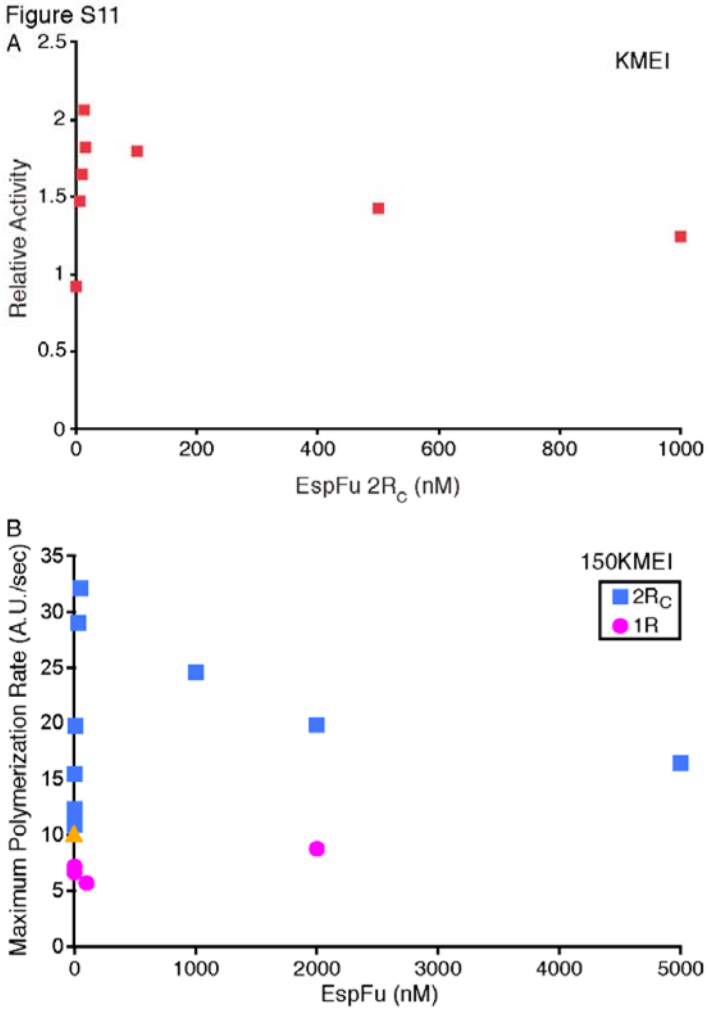

Figure S11. EspFu 2R$_C$ hyperactivates N-WASP$_C$.

Quantified activation of N-WASP$_C$ by 2R$_C$ in KMEI and 150KMEI. (A) Relative activity of 25 nM N-WASP$_C$ plus increasing concentrations of 2R$_C$, performed in KMEI buffer. **(**B**)** The maximum polymerization rates derived from Arp2/3-mediated actin assembly assays in the presence of 100 nM N-WASP$_C$ plus increasing concentration of EspFu 2R$_C$. Data shown for EspFu 2R$_C$ (blue square) or 1R (magenta circle) in 150KMEI. Orange triangle shows the maximum polymerization rate induced by Arp2/3 complex and 100 nM N-WASP VCA.

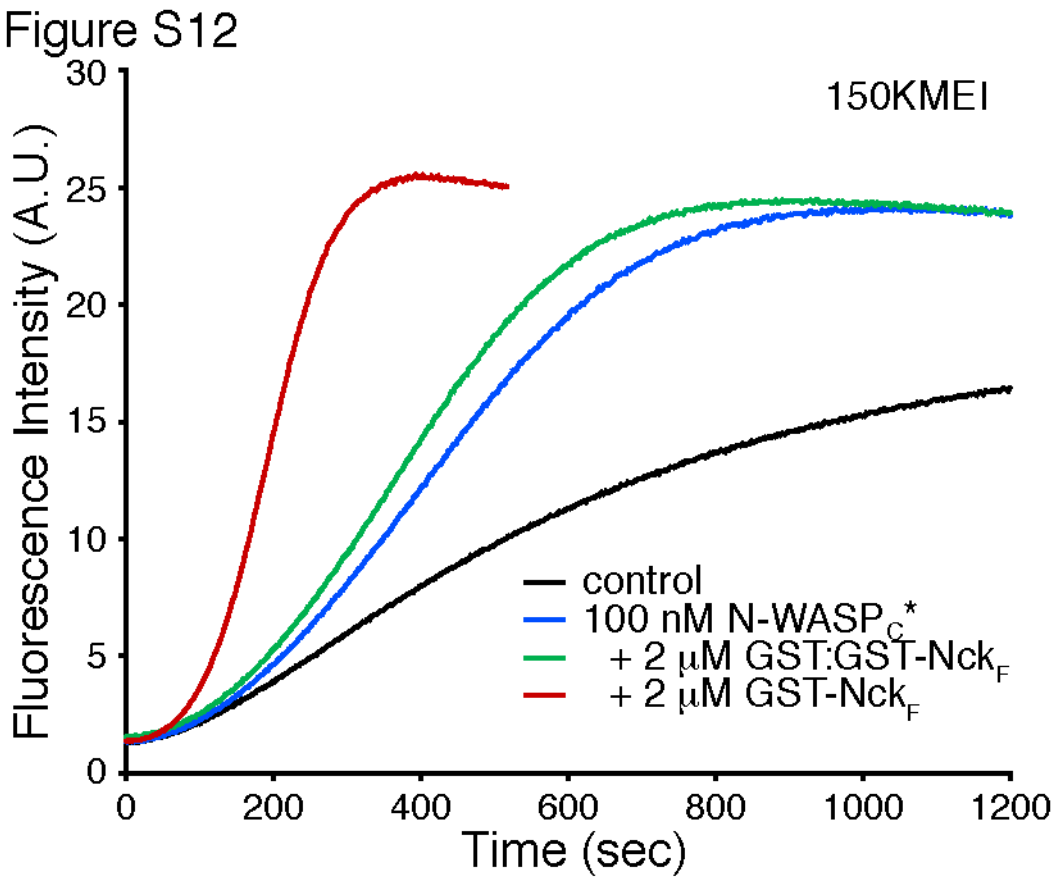

Figure S12. Homodimeric GST-Nck$_F$ hyperactivates N-WASP$_C$*.

Pyrene-actin fluorescence measured during Arp2/3-mediated actin assembly (black) in the presence of 100 nM N-WASP$_C$* (blue); 100 nM N-WASP$_C$* + 2 μM GST:GST-Nck$_F$ heterodimer (green); 100 nM N-WASP$_C$* + 2 μM GST-Nck$_F$ homodimer (red). Assays performed in 150KMEI.

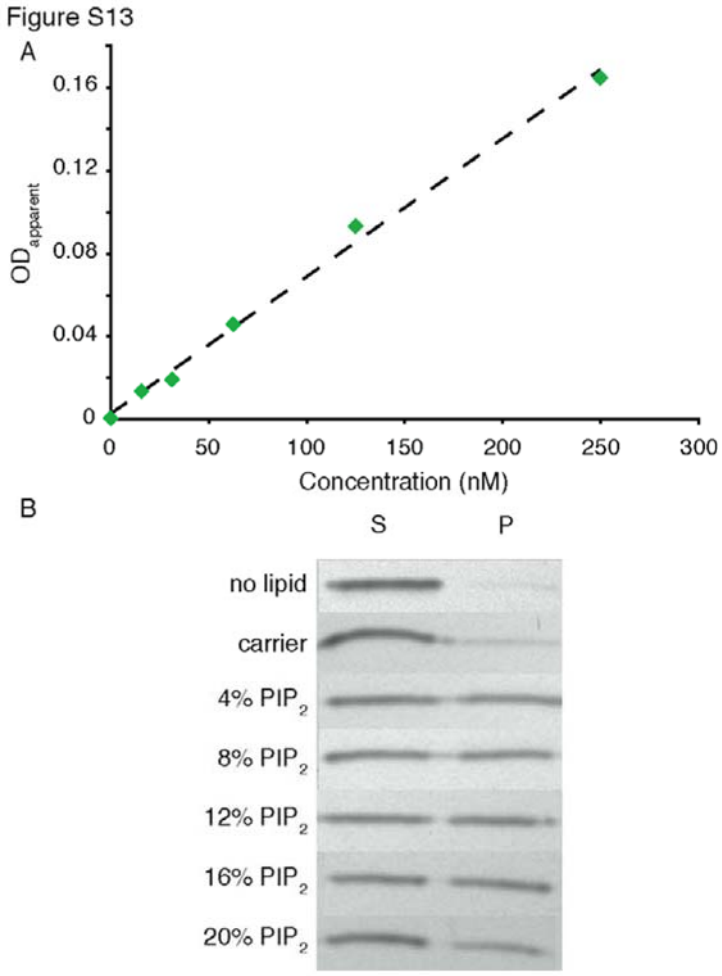

Figure S13. Quantitation of Cosedimentation Assay.

(A) Silver stained SDS-PAGE band intensity is linear over the concentrations used in the cosedimentation experiment. Known quantities of N-WASP$_B$ were loaded on an SDS-PAGE gel, silver stained and the resulting bands were quantified using NIH ImageJ. Apparent OD measured for each band is linear between 40 and 200 nM. (B) Representative bands for supernatant (S) and pellet (P) fractions of N-WASP$_B$ cosedimentation with the indicated vesicles.

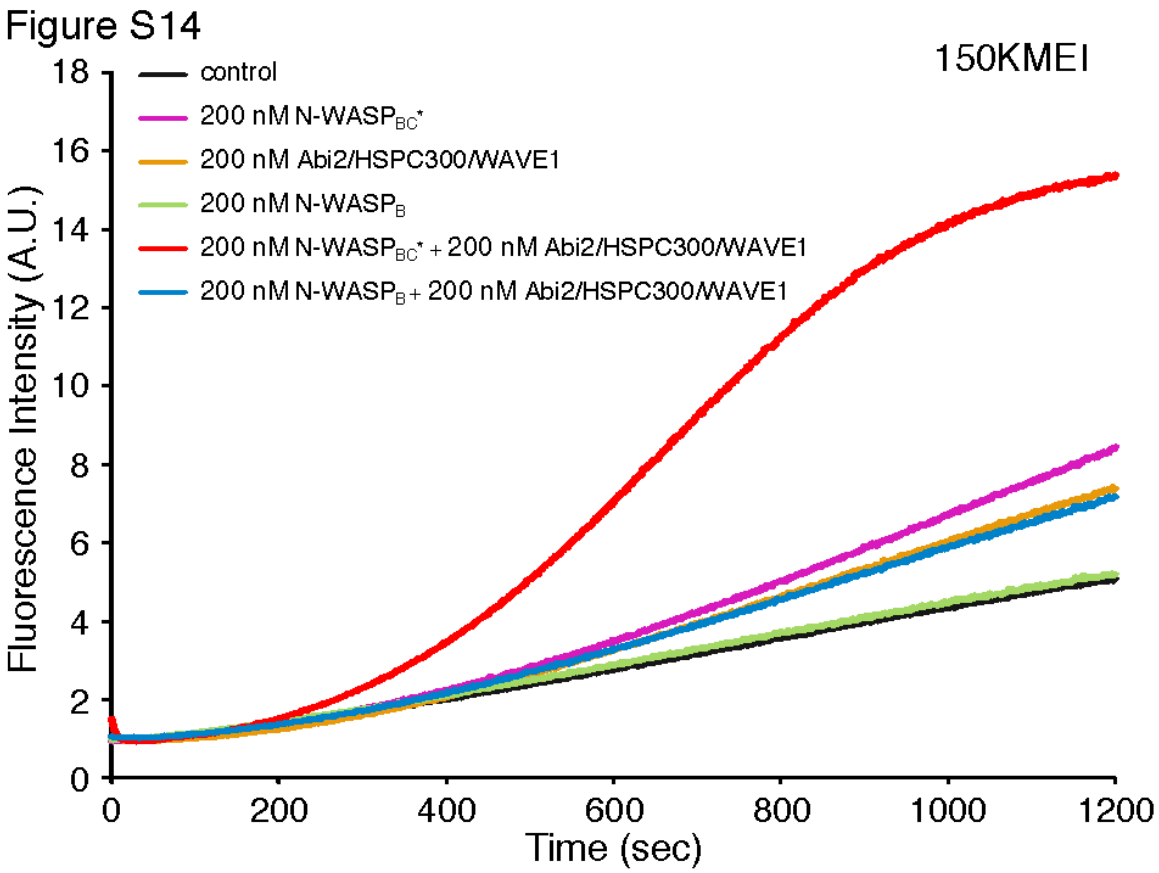

Figure S14. Heterodimerization of N-WASP and WAVE1 hyperactivates Arp2/3.

Pyrene-actin fluorescence measured during Arp2/3-mediated actin assembly (black) in the presence of 200 nM N-WASP$_{BC}$* (magenta), 200 nM Abi2-HSPC-WAVE1 trimer (orange), 200 nM N-WASP$_{B}$ (green), 200 nM N-WASP$_{BC}$* + 200 nM Abi2-HSPC-WAVE1 (red), 200 nM N-WASP$_{B}$ + 200 nM Abi2-HSPC-WAVE1 (blue). Assays performed in 150KMEI.

SUPPLEMENTAL REFERENCES

Brown, P. H., and Schuck, P. (2006). Macromolecular size-and-shape distributions by sedimentation velocity analytical ultracentrifugation. Biophys J *90*, 4651-4661.

Cheng, H.-C., Skehan, B. M., Campellone, K. G., Leong, J. M., and Rosen, M. K. (2008). Structural Mechanism of WASP Activation by the Enterohaemorrhagic E. Coli Effector EspFu. Nature *454*, 1009-13.

Cooper, J. A., and Pollard, T. D. (1982). Methods to measure actin polymerization. Methods Enzymol *85 Pt B*, 182-210.

Dam, J., Velikovsky, C. A., Mariuzza, R. A., Urbanke, C., and Schuck, P. (2005). Sedimentation velocity analysis of heterogeneous protein-protein interactions: Lamm equation modeling and sedimentation coefficient distributions c(s). Biophys J *89*, 619-634.

Devore, J. L. (2000). Probability and statistics for engineering and the sciences (Pacific Grove, CA: Duxbury).

Devriendt, K., Kim, A. S., Mathijs, G., Frints, S. G., Schwartz, M., Van Den Oord, J. J., Verhoef, G. E., Boogaerts, M. A., Fryns, J. P., You, D., *et al.* (2001). Constitutively activating mutation in WASP causes X-linked severe congenital neutropenia. Nat Genet *27*, 313-317.

Fujiwara, I., Vavylonis, D., and Pollard, T. D. (2007). Polymerization kinetics of ADP-and ADP-Pi-actin determined by fluorescence microscopy. Proc Natl Acad Sci U S A *104*, 8827-8832.

Higgs, H. N., Blanchoin, L., and Pollard, T. D. (1999). Influence of the C terminus of Wiskott-Aldrich syndrome protein (WASp) and the Arp2/3 complex on actin polymerization. Biochemistry *38*, 15212-15222.

Ho, H. Y., Rohatgi, R., Lebensohn, A. M., and Kirschner, M. W. (2006). In vitro reconstitution of cdc42-mediated actin assembly using purified components. Methods Enzymol *406*, 174-190.

Kim, A. S., Kakalis, L. T., Abdul-Manan, N., Liu, G. A., and Rosen, M. K. (2000). Autoinhibition and activation mechanisms of the Wiskott-Aldrich syndrome protein. Nature *404*, 151-158.

Ladbury, J. E., Lemmon, M. A., Zhou, M., Green, J., Botfield, M. C., and Schlessinger, J. (1995). Measurement of the binding of tyrosyl phosphopeptides to SH2 domains: a reappraisal. Proc Natl Acad Sci U S A *92*, 3199-3203.

Laue, T. M., Shah, B. D., Ridgeway, R. M., and Pelletier, S. L. (1992). Computer-aided interpretation of analytical sedimentation data for proteins, In Analytical Ultracentrifugation in Biochemistry and Polymer Science, S. E. Harding, A. J. Rowe, and J. C. Horton, eds. (Cambridge, UK: The Royal Society of Chemistry).

Leung, D. W., Morgan, D. M., and Rosen, M. K. (2006). Biochemical properties and inhibitors of (N-)WASP. Methods Enzymol *406*, 281-296.

Marchand, J. B., Kaiser, D. A., Pollard, T. D., and Higgs, H. N. (2001). Interaction of WASP/Scar proteins with actin and vertebrate Arp2/3 complex. Nat Cell Biol *3*, 76-82.

Panchal, S. C., Kaiser, D. A., Torres, E., Pollard, T. D., and Rosen, M. K. (2003). A Conserved Amphipathic Helix in WASP/Scar Proteins is Essential for Activation of Arp2/3 Complex. Nat Struct Biol *10*, 591-598.

Schuck, P. (2000). Size-distribution analysis of macromolecules by sedimentation velocity ultracentrifugation and lamm equation modeling. Biophys J *78*, 1606-1619.

Zalevsky, J., Lempert, L., Kranitz, H., and Mullins, R. D. (2001). Different WASP family proteins stimulate different Arp2/3 complex- dependent actin-nucleating activities. Curr Biol *11*, 1903-1913.